VHF/UHF Imagery and RCS Measurements of Ground Targets in Forested Terrain

A. J. Gatesman[*a], C. Beaudoin[a], R. H. Giles[a], J. Waldman[a], and W. E. Nixon[b]

[a]Submillimeter-Wave Technology Laboratory, University of Massachusetts Lowell
Lowell, MA 01854

[b]U.S. Army National Ground Intelligence Center, 2055 Boulders Road
Charlottesville, VA 22911

ABSTRACT

The monostatic VV and HH-polarized radar signatures of several targets and trees have been measured at foliage penetration frequencies (VHF/UHF) by using 1/35th scale models and an indoor radar range operating at X-band. An array of high-fidelity scale model ground vehicles and test objects as well as scaled ground terrain and trees have been fabricated for the study. Radar measurement accuracy has been confirmed by comparing the signature of a test object with a method of moments radar cross section prediction code. In addition to acquiring signatures of targets located on a smooth, dielectric ground plane, data have also been acquired with targets located in simulated wooded terrain that included scaled tree trunks and tree branches. In order to assure the correct backscattering behavior, all dielectric properties of live tree wood and moist soil were scaled properly to match the complex dielectric constant of the full-scale materials. The impact of the surrounding tree clutter on the VHF/UHF radar signatures of ground vehicles was accessed. Data were processed into high-resolution, polar-formatted ISAR imagery and signature comparisons are made between targets in open-field and forested scenarios.

Keywords: VHF, UHF, radar, signature, trees, imagery, decoy

1. INTRODUCTION

For the past twenty years, Expert Radar Signature Solutions (ERADS) under funding from the National Ground Intelligence Center (NGIC) has developed state-of-the-art scale model measurement systems to acquire radar signatures in support of a number of advanced radar applications such as automatic target recognition (ATR) systems, low-observable target evaluation, RAM development, and buried object detection. ERADS has developed fully polarimetric compact ranges at 160 GHz[1], 520 GHz[2], and, 1.56 THz[3] for acquisition of X-band, Ka-band, and W-band radar imagery of 1/16th and 1/48th scale model targets and scenes.

[*] correspondence: email: andrew_gatesman@uml.edu; telephone: 978-458-3807; fax: 978-452-3333; web: http://stl.uml.edu;
mail: Submillimeter-Wave Technology Laboratory, 175 Cabot Street, Suite 130, Lowell, MA 01854

Report Documentation Page

Public reporting burden for the collection of information is estimated to average 1 hour per response, including the time for reviewing instructions, searching existing data sources, gathering and maintaining the data needed, and completing and reviewing the collection of information. Send comments regarding this burden estimate or any other aspect of this collection of information, including suggestions for reducing this burden, to Washington Headquarters Services, Directorate for Information Operations and Reports, 1215 Jefferson Davis Highway, Suite 1204, Arlington VA 22202-4302. Respondents should be aware that notwithstanding any other provision of law, no person shall be subject to a penalty for failing to comply with a collection of information if it does not display a currently valid OMB control number.

1. REPORT DATE **AUG 2002**	2. REPORT TYPE	3. DATES COVERED **00-00-2002 to 00-00-2002**

4. TITLE AND SUBTITLE **VHF/UHF Imagery and RCS Measurements of Ground Targets in Forested Terrain**	5a. CONTRACT NUMBER
	5b. GRANT NUMBER
	5c. PROGRAM ELEMENT NUMBER
6. AUTHOR(S)	5d. PROJECT NUMBER
	5e. TASK NUMBER
	5f. WORK UNIT NUMBER

7. PERFORMING ORGANIZATION NAME(S) AND ADDRESS(ES) **University of Massachusetts Lowell,Submillimeter-Wave Technology Laboratory,175 Cabot Street,Lowell,MA,01854**	8. PERFORMING ORGANIZATION REPORT NUMBER

9. SPONSORING/MONITORING AGENCY NAME(S) AND ADDRESS(ES)	10. SPONSOR/MONITOR'S ACRONYM(S)
	11. SPONSOR/MONITOR'S REPORT NUMBER(S)

12. DISTRIBUTION/AVAILABILITY STATEMENT
Approved for public release; distribution unlimited

13. SUPPLEMENTARY NOTES
The original document contains color images.

14. ABSTRACT

15. SUBJECT TERMS

16. SECURITY CLASSIFICATION OF:			17. LIMITATION OF ABSTRACT	18. NUMBER OF PAGES	19a. NAME OF RESPONSIBLE PERSON
a. REPORT **unclassified**	b. ABSTRACT **unclassified**	c. THIS PAGE **unclassified**		**11**	

Recently, there has been an increase in interest in developing systems capable of detecting and identifying threat military targets under trees. Such foliage penetration (FOPEN) systems typically rely on low frequencies (f < 1 GHz) to penetrate forest canopies and large bandwidths ($\Delta f \approx 100\%$) coupled with large synthetic apertures (20°-60° aspect swaths) to achieve ≈ 1 sq. meter resolution cells. In addition to forest canopy penetration, operation at low frequencies also reduces radar backscatter from small branches and rough terrain. However, image resolution is still very low (< 50 resolution cells on target) and tree trunks still remain as large scatterers. As a result, many foliage penetration programs are concentrating on studying backscattering characteristics of the trees themselves.

In response to the growing interest in the problem of detecting and identifying targets under trees, STL has initiated a scale modeling program aimed at gathering radar scattering characteristics of targets in forested areas. STL has developed[4], with NGIC and AFRL (Hanscom AFB, MA) funding, a capability for measuring target signatures at VHF/UHF frequencies using an 8.2-12.4 GHz radar system and 1/35th scale model vehicles. This system, along with STL's capability to develop dielectrically scaled ground terrain and trees was used to acquire the monostatic VV and HH-polarized radar signatures of several ground targets in forested terrain at foliage penetration frequencies. This paper describes STL's current capabilities to measure and analyze VHF/UHF radar signatures of targets located in forested scenes and potential uses of such a system to study the FOPEN problem in general.

2. MEASUREMENT SYSTEM AND SCALE MODELS

The measurement system used to acquire the target's radar signatures consisted of a microwave transceiver, target/calibration positioning stage, and a data acquisition and processing computer. The scale model radar range is shown in Figure 1. The transceiver was based on a Hewlett-Packard microwave network analyzer. The system consisted of a HP8341B microwave source, HP8516A S-parameter test set, and a HP8510B network analyzer. Though the system was not intended for use as a radar transceiver (no pulsing capability, modest dynamic range, etc.) it was sufficient for measuring the radar cross sections of 1/35th scale models.
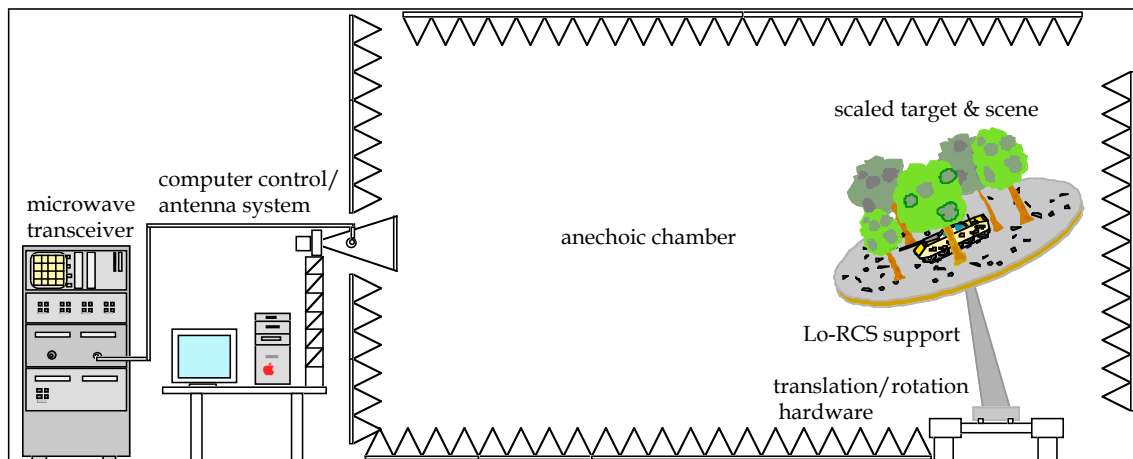

Figure 1. Configuration of the X-band radar system used for acquisition of VHF/UHF signatures of 1/35th scale models.

System Hardware and Measurement Procedure-

Port 1 of the S-parameter test set was connected with rigid waveguide to a 12–inch-diameter Alpha Industries spot–focusing conical horn antenna designed for use between 8.2 and 12.4 GHz. Though the HP8510B can operate between 40 MHz and 40 GHz, the waveguide/horn combination limited the frequency of operation to X-band. The hyperbolic/spherical lens at the horn's aperture was modified to a hyperbolic/flat to produce a gaussian beam waist at the horn's aperture. The combination of the modified lens and horn aperture resulted in a $\approx$ 4.3-in.-radius gaussian beam waist ($1/e^2$ power) at the horn's output aperture. The radiation was allowed to expand as a spherical-gaussian beam out to the target under test. The target was placed in the far-field ($2D^2/\lambda \approx$ 25 ft.) of the transmitting horn. A 4-axis computer-controlled stage was used to control the position of the target and calibration object as needed. Three axes controlled the translation, azimuth, and elevation of the ground plane / target scene and the forth axis was used to position a flat plate used for calibration.

Target measurement involved stepping the transmitted frequency over the required bandwidth while the receiver recorded the magnitude and phase of the backscattered signal at each frequency step. The procedure was repeated for each desired azimuthal angle of the target and scene. Prior to acquiring data on a target, a background frequency sweep was collected with the target and calibration plate both removed from the chamber. Next, a flat plate of known radar cross section was then translated into the beam and a second frequency sweep was acquired. The background sweep was then coherently subtracted from the flat plate data. The plate data (with background now removed) were compared to their theoretical response and used to obtain a normalization array, which was subsequently applied to each target frequency sweep. Finally, a correction for the beam divergence was applied to the data to account for the fact that the target and calibration plate were at different distances from the radar during measurement. The result was a fully calibrated frequency sweep. Prior to image processing, software range gating was applied to the calibrated frequency data. Acquiring data over 801 frequency points over a 4.2 GHz bandwidth allowed the entire measurement chamber to be resolved in range so that unwanted scattering from the transmitting horn, lens, back wall, etc. could be removed.

Scale Model Target and Scenes-

Four individual $1/35^{th}$ scale targets and three types of trees were used in the VHF/UHF measurement study. The targets (Figure 2) consisted of an M1 tank, an M-47 tank, a rectangular block machined to approximatly the same size as a scale model tank (2.25"x4"x8"), and a tank decoy. The tree targets consisted of a simple tree trunk, a 6-branch tree, and a 120-branch tree. The M1 was coated with $\approx$ 4000 Å of copper and the M-47 was coated with $\approx$ 2000"Å of aluminum. Assuming that the metal film resistivities were no more than 10x higher than their bulk values, the X-band reflectivities were $\geq$99% and $\geq$98%, respectively. A full-scale tank decoy was assumed to be approximatly the same size as a tank and built from 2 x 4 lumber and metallic wire mesh. A scale model was constructed using balsa wood to simulate the dielectric behavior of construction lumber and a metal mesh of the appropriate aperture size. Measurements were acquired for each target on a ground plane with and without an arrangement of 8 120-branch trees. Figure 3 shows the M1 tank located in an array of 8 trees on the dielectric ground plane. The two simpler trees (tree trunk and 6-branch tree) were measured individually without other targets present. All measurements were acquired over a 360° azimuth spin and at 45° elevation. The dielectric properties of live tree wood and moist soil were properly scaled to X-band. Dielectric scaling[5,6] requires that the complex dielectric constant of tree wood and moist soil at VHF/UHF frequencies match the scale model materials at X-band. An aluminum-loaded epoxy ($\varepsilon \approx$ 69 + i"10 at 10 GHz) was used to simulate the properties of live wood and a graphite-loaded polyurethane resin ($\varepsilon \approx$ 14 + i 1.4 at 10 GHz) was used to model soil.
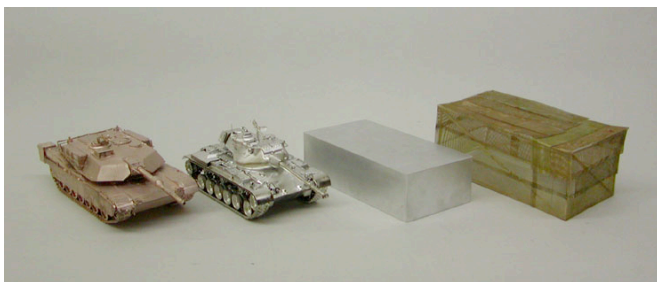
Figure 2a. The four 1/35th scale targets used in the signature study. left to right: M1 tank, M-47 tank, Al block, tank decoy.

Figure 2b. The three tree targets used in the study. left to right: tree trunk, 6-branch tree, 120-branch tree.
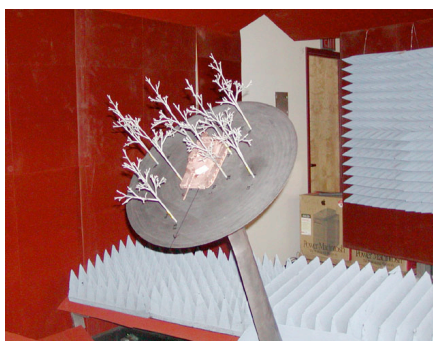

Figure 3. Scale model M1 tank in measurement configuration on the 24"-diameter ground plane with eight trees.

3. DATA VALIDATION

Data validation was performed by making a series of measurements on various flat plates as well as on a metallic test object known as Slicy. A flat rectangular plate (8 in. x 6.125 in.) was mounted in the test range normal to the incident radiation (0° azimuth, 0° elevation) and rotated in azimuth over an extent of ± 35° while maintaining a fixed elevation angle of 0°. RCS data were then compared with a geometrical theory of diffraction (GTD) prediction. Excellent agreement was observed between the X-band data and the GTD prediction. Figure 4 shows the data and the GTD prediction at 8.2 and 12.4 GHz.
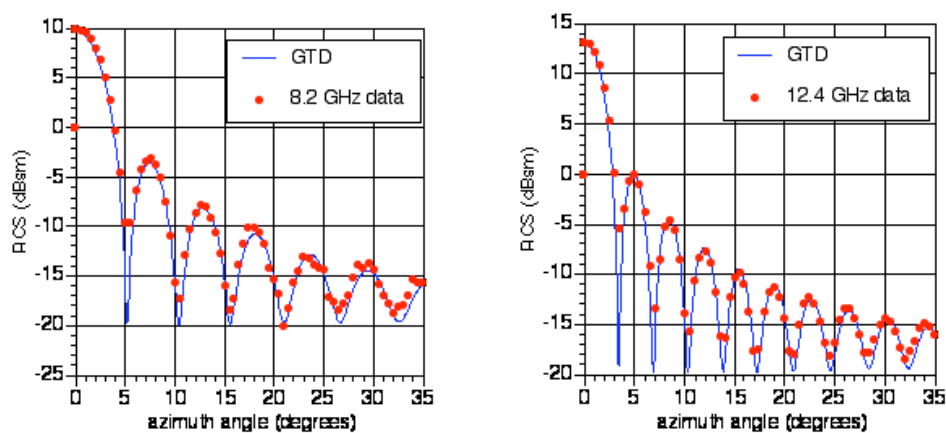

Figure 4. RCS data and GTD prediction of an 8 in. x 6.125 in. flat plate as a function of azimuth at 0° elevation.

As a second validation test of the data, RCS measurements were acquired on a metallic scale model of a target know as Slicy (Figure 5) that is comprised of a variety of simple shapes such as dihedrals, trihedrals, and cylinders. A method of moments electromagnetics prediction code (Carlos) was used to predict the X-band RCS of the target for comparison with laboratory measurements. The Slicy was mounted on a low-RCS pylon at 15° elevation and its X-band RCS was measured over a 360° azimuth sweep. VV and HH-polarized RCS data are shown in Figure 6 below. Excellent agreement was observed between data and the method of moments prediction for both VV and HH polarizations.
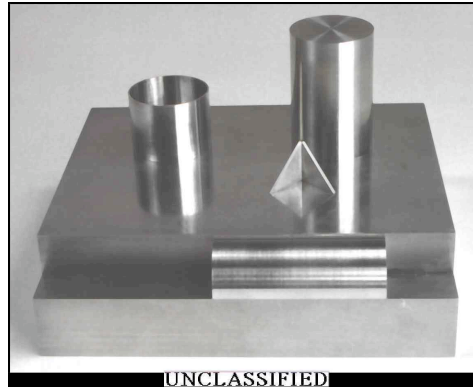

UNCLASSIFIED

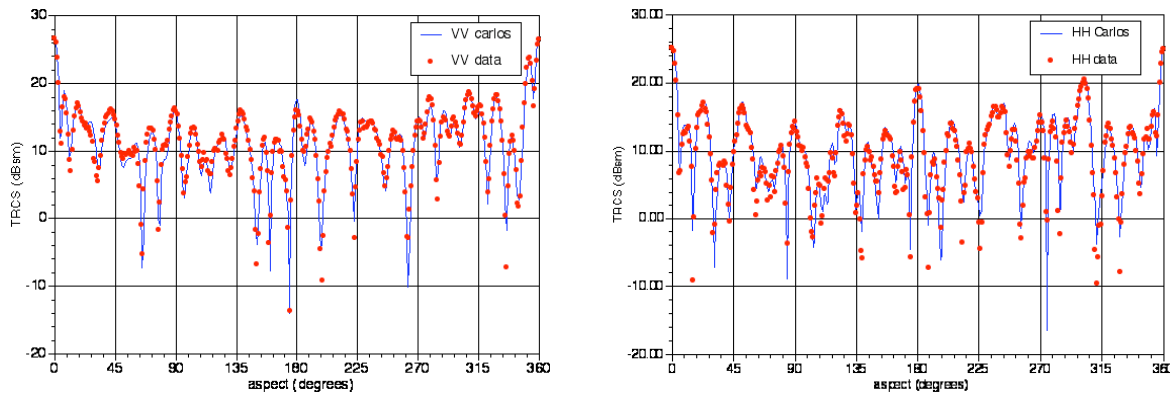Figure 5. Scale model Slicy used to validate the X-band measurement capability.

Figure 6. VV and HH 10 GHz RCS of Slicy. The data have been adjusted to represent VHF/UHF data assuming the model in Fig. 5 was a 1/35th scale Slicy (i.e. $10\log(35^2)$ was added to the measured RCS).

4. IMAGE PROCESSING

This section describes the synthetic aperture processing technique used to form two-dimensional images of objects measured in the FOPEN radar range. In general, radar imaging systems collect coherent reflectivity data $G(\theta,f)$ from a target as a function of frequency over bandwidth β and target rotation angle Δθ. Fourier transforms can then be applied to the data to obtain the target's reflectivity density function, g(x,y). The distribution of scatterers in the range

direction can be obtained from a one-dimensional Fourier transform of G(θ,f) applied in the frequency direction. A subsequent one-dimensional Fourier transform can then be applied in the θ direction to obtain cross-range information. Therefore, two one-dimensional transforms can be used to find the target's reflectivity function g(x,y). Arbitrarily high range resolution (δr = c/2β) can be obtained by increasing the bandwidth β. Increased cross-range resolution (λ/(2sinΔθ) can be obtained by increasing the range of angles over which the cross-range Fourier transform is processed. However, the Fourier transform used to obtain cross-range data is only an approximation of the exact computation necessary to achieve optimal cross-range resolution. ISAR imagery processed using Fourier transforms; one in frequency to obtain range, and one in angle to obtain cross-range ignores the coupling between range and cross-range induced by the rotational motion of the target over large angular sweeps and therefore results in an unfocused image. The extent of the blurring depends on both the target size and wavelength.

In order to form an X-band image of a ≈ 24"-diameter scene with reasonable resolution (≈ 1 sq. in. resolution cells), a 4 GHz frequency bandwidth and ≈ 35° angular swaths of data were used. Coherent processing over such a large region in the data domain requires the use of focusing techniques, which, if not used, would result in a blurred image when the data is transformed into the image domain. The following section describes the specific focusing algorithm[7] used as well as the approximations made when the algorithm is not used.

Consider a set of fixed point scatterers with coordinates x,y, (or r,ψ in polar coordinates). Assume a radar system is free to rotate to any angle θ around the target-fixed coordinate system. The amplitude and phase measured by the radar at a given radar position θ and frequency f is given by:

$$G(\theta,f) = \sum_x \sum_y g(x,y) \ \exp[\ j\frac{4\pi fr}{c} \sin(\psi + \theta)]. \qquad Eq.(1)$$

By expanding the sin(ψ+θ) term, Eq. (1) can be written as:

$$G(\theta,f) = \sum_x \sum_y g(x,y) \ \exp[\ j\frac{4\pi fr}{c}(\sin\psi\cos\theta + \cos\psi\sin\theta)]. \quad Eq.(2)$$

Inserting the expressions for the x and y scatterers (x = r cosψ and y = r sinψ) gives:

$$G(\theta,f) = \sum_x \sum_y g(x,y) \ \exp[\ j2\pi(\frac{2fx}{c}\sin\theta + \frac{2fy}{c}\cos\theta)]. \quad Eq.(3).$$

When image processing is confined to small angular swaths, Eq. (3) can be simplified to:

$$G(\theta,f) = \sum_x \sum_y g(x,y) \ \exp[\frac{j4\pi}{c}(f_0x\theta + fy)]. \quad Eq.(4).$$

A 2-dimensional Fourier transform can then be applied to Eq. (4) to give the reflectivity density (an image) of the target:

$$g(x,y) = \sum_f \sum_\theta G(\theta,f) \ \exp[-\ j\frac{4\pi}{c}(f_0x\theta + fy)]. \quad Eq.(5).$$

Eq. (5) represents the expression used for unfocused ISAR processing. It ignores the coupling between range and cross-range resulting from the rotational motion of the target. However, note that the complex exponential can be written as the product of two functions, one for θ and one for f. This feature allows the Fourier processing to consist of two separate one-dimensional Fourier transforms that can be applied independently over θ and f and thus allows windowing functions to be used to minimize sidelobes. In addition, since the frequency domain data are assumed to exist on a uniformly spaced (rectangular) grid, the fast-Fourier transform can be utilized for computational speed.

When image processing over wide angular extents and bandwidths such as in this research, Eq. (5) can no longer be used to generate reasonably focused imagery. By defining two new spatial spectrum variables as $X = 2(f/c)\sin\theta$ and $Y = 2(f/c)\cos\theta$, Eq. (3) can be rewritten:

$$G(\theta,f) = \sum_x \sum_y g(x,y) \; \exp[\,j2\pi(Xx+Yy)]. \quad Eq.(6).$$

A 2-dimensional Fourier transform can then be applied to Eq. (6) to find a focused estimate of the target's reflectivity function.

$$g(x,y) = \sum_f \sum_\theta G(\theta,f) \; \exp[-\,j2\pi(Xx+Yy)]. \quad Eq.(7).$$

The complex exponential in Eq. (7) correctly compensates for the fact that G(θ,f) is acquired over large areas in the frequency domain thus Eq. (7) can be used to produce focused ISAR imagery. It is a focusing algorithm because it correctly compensates for the phase of a scatterer as it moves in a circular (opposed to linear) trajectory. For small angular rotations, target scatterers can be considered to move in straight trajectories and therefore need no focusing and Eq. (4) can be used. Note, however, that the complex exponential in Eq. (7) can no longer be written as the product of two functions (one for θ and one for f) as was possible in Eq. (5), and therefore effective windowing functions to minimize sidelobes are more difficult to apply to f and θ independently. In addition, due to the fact that G(θ,f) data exists on a polar raster, the fast-Fourier transform, which assumes uniformly-spaced arrays, can no longer be used.

5. VHF/UHF MEASUREMENTS

Each measurement of the vehicles (with and without trees) was acquired at 45° elevation and over a 360° azimuth spin. For each azimuth look angle, the frequency was stepped between 8.2 GHz and 12.4 GHz (234 MHz - 354 MHz full-scale). Acquiring data over a wide range of frequencies at each azimuth angle allows for calculation of a frequency-averaged radar cross section. Table I is a summary of all data acquired. The data are expressed as the total radar cross section (TRCS) which is defined here as the median of the frequency averaged data. A number of interesting features can be observed from the tabulated data. First, notice that the decoy's TRCS is within ≈1 dB of both the M-47's and the M1's cross section indicating that the shape and materials of the decoy were properly chosen. Secondly, the 6–branch tree had a TRCS that was only slightly greater than the tree trunk data. The fact that the VV increase (2.6 dB) was more pronounced than HH (0.2 dB) was probably due to the fact that the majority of the scatterers on the 6-branch tree are predominately vertically oriented. In addition, the TRSC of the 120-branch tree increased only slightly over the 6-branch tree indicating that the majority of the tree scattering originated from the relatively few large branches and trunk. This result gives some indication that small and medium sized branches do not contribute significantly to the 234-354 MHz cross section of a tree. It is interesting to note that a tree trunk has a TRCS that is as high as a tank at these frequencies.

Table I. VHF/UHF TRCS of several targets and trees.

	free space	ground plane w/o trees	ground plane with trees	trees only
M1 tank	10.2 VV 10.0 HH	10.7 VV 11.8 HH	19.5 VV 19.8 HH	-
M-47 tank	8.8 VV 7.7 HH	9.4 VV 11.2 HH	19.3 VV 19.5 HH	-
Slicy	15.5 VV 15.1 HH	16.3 VV 15.6 HH	19.4 VV 19.9 HH	-
Al block	-	7.5 VV 8.7 HH	20.7 VV 20.0 HH	-
tank decoy	-	9.5 VV 11.8 HH	21.1 VV 20.4 HH	-
8 120-branch trees	-	-	-	19.3 VV 19.4 HH
1 120-branch tree	-	-	-	13.5 VV 13.6 HH
1 6-branch tree	-	-	-	13.3 VV 12.2 HH
1 tree trunk	-	-	-	10.7 VV 12.0 HH

For three of the vehicles (M1 tank, M-47 tank, and Slicy), free-space measurements were also acquired to access the impact of the ground plane on the TRCS. In each case, there was only a modest increase in the signature when placed on a smooth dielectric ground plane simulating soil with some moisture. The impact of the ground plane (without trees) can be seen in Figure 7 where the TRCS of the M1 tank is plotted as a function of azimuth angle. The signature was impacted the most at the cardinal angles, however, the median cross section does not significantly increase when placed on the ground plane.
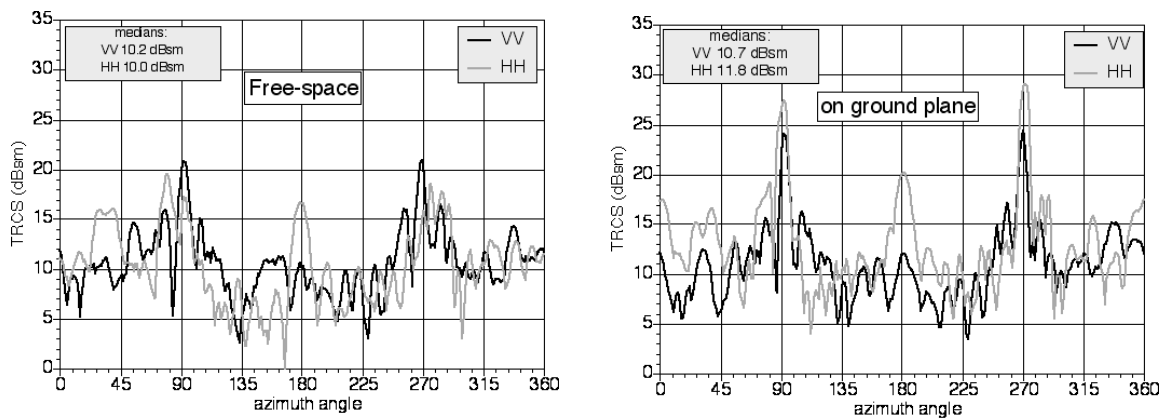

Figure 7. VHF/UHF TRCS of an M1 tank in both a free-space configuration and on a ground plane without trees.

The impact of the trees on the signature of the M1 tank is shown in Figure 8 below. A single tree, as noted above, has a TRCS at VHF/UHF frequencies that is similar to a tank. Notice that at the cardinal angles, only the HH signature survives when trees surround the M1 tank.
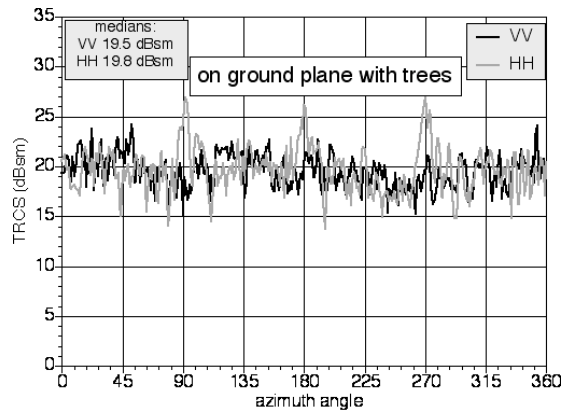
Figure 8. VHF/UHF TRCS of an M1 tank on a ground plane with eight 120-branch trees.

By generating ISAR imagery as described by Eq (7), the impact of the trees can be assessed. All imagery described here have been processed over a 36° azimuthal sweep and over a 120 MHz bandwidth resulting in a 1.25 m range resolution and 1 m cross-range resolution (full-scale). In the imagery shown here, black represents a cross section of -15 dBsm and white is -30 dBsm (or lower). Each image is made up of 100 x 100 pixels and the x and y axes have units of cm. Figure 9 shows the VV and HH signatures of the 8 trees used in the study. The image is centered around 302° azimuth and the location of all 8 trees can easily be observed.
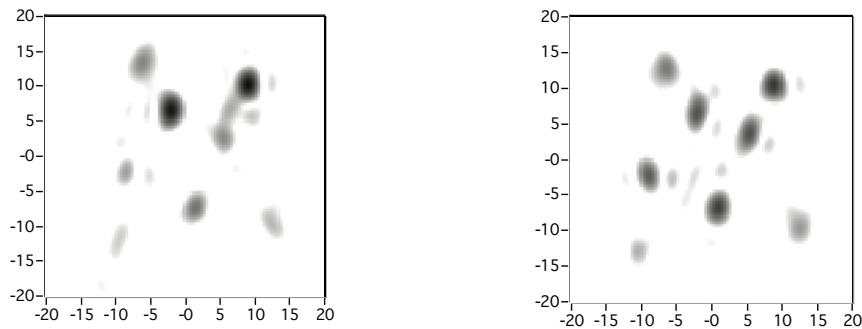

Figure 9. ISAR imagery (VV left, HH right) of 8 scale model trees on a ground plane.

Imagery was also generated for the M1 tank located in the group of 8 trees. Figures 10 and 11 compare the images of the M1 tank in trees to a corresponding image without trees at a 90° center azimuth angle. To some extent, the trees have a lesser impact on the HH signature than the VV. This can more easily be observed in the Al block data.
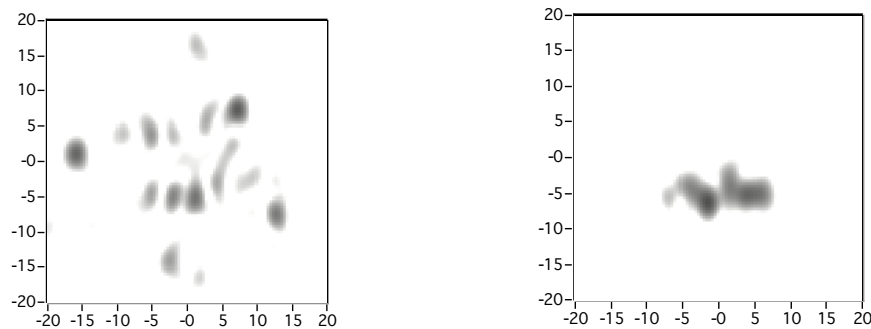

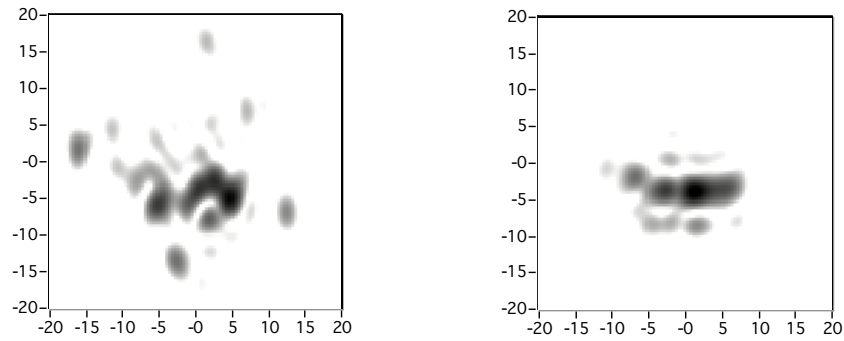Figure 10. VV ISAR imagery of M1 tank in trees (left) and M1 tank without trees (right).

Figure 11. HH ISAR imagery of M1 tank in trees (left) and M1 tank without trees (right).

Figure 12 shows the result of the aluminum block (at 90° center azimuth angle) where the trees-only data have been incoherently subtracted out. The HH block image is better preserved than the corresponding VV image and most likely due to the greater attenuating and scattering that occurs with the VV radiation which is polarized in the direction of the tree trunks and the majority of the branches.
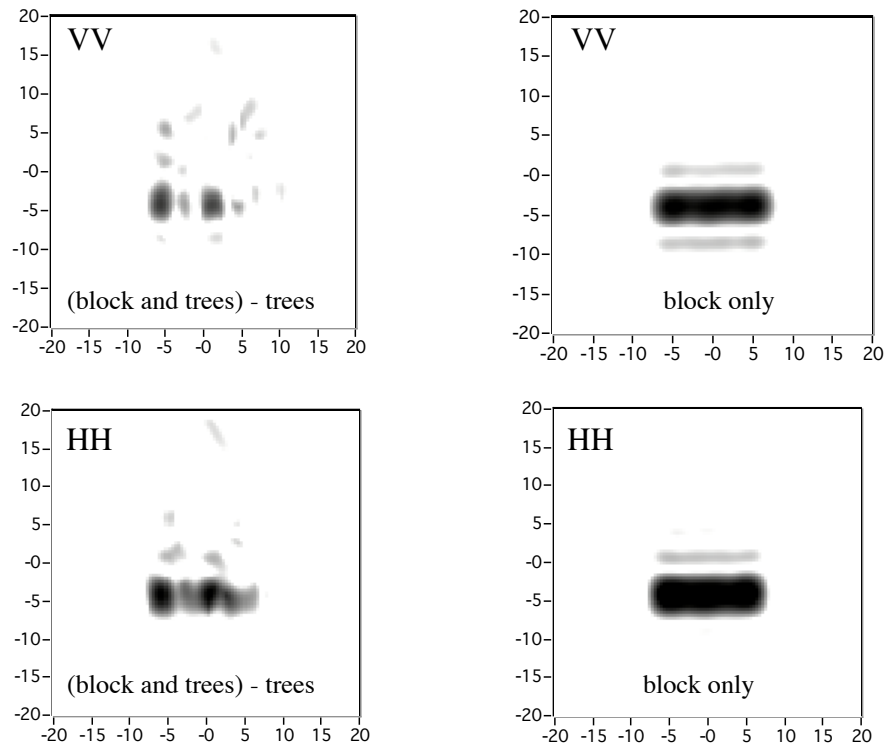

Figure 12. ISAR imagery of the aluminum block where the trees-only data have been incoherently subtracted out demonstrating how the HH image is better preserved when the target is obscured by predominately vertical scatterers.

6. CONCLUSION

A polarimetric measurement system capable of acquiring calibrated VHF/UHF radar cross sections and ISAR imagery of targets has been developed. A method of moments code has been used to establish the validity of the signature measurements. Dielectric scaling technology has been used to fabricate simulated ground terrain as well as several trees and thus enabled the radar characterization of targets located in forested terrain. The impact of the smaller and mid-sized branches on the radar cross section of a tree has been studied. ISAR imagery has been generated of targets located in forested areas. The VV signature of a target appears to be influenced more by the trees than the HH signature.

ACKNOWLEDGEMENTS

REFERENCES

1. M. J. Coulombe, T. Horgan, J. Waldman, J. Neilson, S. Carter, and W. Nixon, "A 160 GHz Polarimetric Compact Range for Scale Model RCS Measurements," Antenna Measurements and Techniques Association (AMTA) Proceedings, Seattle, WA, October 1996.

2. M. J. Coulombe, T. Horgan, J. Waldman, G. Scatkowski, and W. Nixon, "A 520 GHz Polarimetric Compact Range for Scale Model RCS Measurements," Antenna Measurements and Techniques Association (AMTA) Proceedings, Monterey, October 1999.

3. T. M. Goyette, J. C. Dickinson, J. Waldman, W. E. Nixon, and S. Carter, "Fully Polarimetric W-band ISAR Imagery of Scale-Model Tactical Targets Using a 1.56 THz Compact Range," Proceeding of SPIE 15th Annual Inter. Symp. on Aerospace/Defense, Simulation, and Controls, Vol. 4382, Orlando, FL, April 2001.

4. C. J. Beaudoin, "Development of a 1/35th Scale VHF/UHF Far-Field RCS Imaging System Used to Investigate Scattering and Imagery of Tree Obscured Targets," M.S. Thesis, University of Massachusetts Lowell, Dec. 2001.

5. R. H. Giles, A. J. Gatesman, J. Fitz-Gerald, S. Fisk, and J. Waldman, "Tailoring Artificial Dielectric Materials at Terahertz Frequencies," The Fourth International Symposium on Space Terahertz Technology, April 1993, Los Angeles, CA.

6. A. J. Gatesman, T. M. Goyette, J. C. Dickinson, J. Waldman, J. Neilson, and W. E. Nixon, "Physical scale modeling the millimeter-wave backscattering behavior of ground clutter," SPIE's 15th Annual Symposium on Aerospace/Defense Sensing, Simulation, and Controls, Orlando, FL, Apr. 2001.

7. D. L. Mensa, High Resolution Radar Cross-Section Imaging, Artech House, Inc. Norwood, MA 1991.